J Nanostruct 16(3): 3311-3322, Summer 2026

RESEARCH PAPER

Laser-Ablated Au-Nanoparticles with Tunable Optical and Antibacterial Properties for Photothermal Antimicrobial Therapy

Sadeq Mohammed Burhan [1], *Taoufik Soltani* [1], *Entidhar Jasim Khamees* [2] *

[1] *Faculty of Sciences, University of Tunis El Manar, Tunisia*

[2] *Department of Physiology and Medical Physics, Babylon University, Iraq*

ARTICLE INFO

Article History:
Received 24 March 2026
Accepted 18 May 2026
Published 01 July 2026

Keywords:
Antibacterial Activity
Laser Irradiation
Nanoparticles (AuNPs)
Photothermal/Plasmonic Synergy
Physical Nanoparticle Synthesis

ABSTRACT

Gold nanoparticles (AuNPs) were prepared successfully as environmentally friendly colloids that contain high purity and no added chemical agents by using pulsed laser ablation in liquid (PLAL) process. Three different types of liquid environments were used for a systematic evaluation in order to assess the physical characteristics: structural, optical, and antibacterial, respectively, of each medium produced by using double-distilled deionized water (DDDW); sodium hydroxide (NaOH); and polyvinylpyrrolidone (PVP). X-ray diffraction (XRD) measurements confirmed that all the prepared AuNPs crystallized in a face-centered cubic (FCC) form, with the smallest crystallite sizes measured for NaOH-synthesized nanoparticles. Transmission electron microscopy (TEM) studies indicated spherical and mostly well spread nanoparticles with average diameters of around 25–39 nm. UV–Visible spectroscopy for optical characterization showed strongly marked surface plasmon resonance (SPR) absorptions of 356–587 nm with significant variation with the synthesis medium. The optical band gap energies, inferred from Tauc plots, were in the range of 3.8 to 4.7 eV, demonstrating robust coupling upon the size and surface electronic structure of nanoparticles. Antibacterial activity of the prepared AuNPs was measured in Gram-negative Escherichia coli and Gram-positive Streptococcus spp. Although green laser irradiation (532 nm, 300 mW) alone resulted in a relatively modest inhibition in bacterial growth, a significantly better antibacterial effect was demonstrated when laser irradiation coupled with AuNP treatment. The synergy behind this effect is due to laser-induced enhancement of bacterial membrane permeability leading to elevated uptake of nanoparticles and subsequent internal cell damage. The dramatically less bacterial viability was also confirmed by ELISA detection at 405 nm, which once again confirmed the drastic reduction in bacterial viability. In general, the results show that AuNPs, formed by PLAL can demonstrate a high antibacterial activity that could be easily enhanced by laser irradiation. The proposed plasmonic nanoparticle–laser synergy showed promise of PLAL-produced AuNPs for applications in photonic and photothermal antibacterial therapy.

How to cite this article
Burhan S., Soltani T., Khamees E. Laser-Ablated Au-Nanoparticles with Tunable Optical and Antibacterial Properties for Photothermal Antimicrobial Therapy. J Nanostruct, 2026; 16(3):3311-3322. DOI: 10.22052/JNS.2026.03.025

* *Corresponding Author Email: med.intidhar.jasim@uobabylon.edu.iq*

INTRODUCTION

Rapidly emerging bacterial strains resistant to standard antibiotics pose a substantial global health challenge, causing rising morbidity, mortality, and healthcare costs worldwide [1–3]. Most infectious diseases, which were formerly treatable with classical antibacterial drugs, now show reduced or even in some cases complete resistance, thus demand is strong for new therapeutic strategies that are not based mainly on classical biochemical inhibition mechanisms [4,5]. Because of this, physical and physicochemical strategies, including photothermal, photodynamic and nanotechnology-based therapies, have emerged as alternative treatments to conventional ones for bacterial infections [6–8]. Metal nanoparticles, especially gold nanoparticles (AuNPs), have attracted considerable attention as nanomaterials by virtue of their special physicochemical features, superior biocompatibility and chemical stability [9,10]. AuNPs have strong interactions with light via surface plasmon resonance (SPR), in which there are collective oscillations of conduction electrons upon exposure to light of a certain wavelength [11]. This means that optical energy can be effectively converted to localized heat and increased electromagnetic fields, resulting in bacterial membrane damage, protein denaturation and intracellular toxicity [12–14]. Consequently, AuNPs are extensively investigated for light-assisted antibacterial therapy as photothermal agents. The antibacterial efficacy of AuNPs is primarily affected by their size, shape, surface chemistry, and purity, in proportion to the synthesis route [15,16]. Most conventional wet-chemical techniques rely on reducing and stabilizing agents that leave residual contaminants on the surfaces of the nanoparticle which may affect biological activity and cytotoxicity [17]. On the other hand, pulsed laser ablation in liquid (PLAL) has appeared as strong physical synthesis process that can generate highly pure nanoparticles without the application of chemical reagents [18–20]. In PLAL, short laser pulses ablate a solid metal target immersed in liquid media resulting in rapid cooling and nucleation of the nanoparticles directly in the liquid medium. Notably, the properties of nanoparticles can be optimized through the control of laser parameters and the type of surrounding liquid [21,22]. It was shown that using AuNPs as components with laser irradiation improves antibacterial activity significantly more than either nanoparticles or laser treatment alone [23–25]. This interaction was considered as synergistic due to the increasing permeability of bacterial membrane through laser, to the enhanced interaction between nanoparticle with cells and a combination of photothermal and photochemical damage mechanisms. Nonetheless, the magnitude of this improvement is strongly dependent on nanoparticle synthesis conditions, irradiation wavelength and power, and specific bacterial type. In this regard, this article examines in a systematic manner the antibacterial effects of AuNPs manufactured via PLAL in 3 diverse liquid media of polymer (polyvinylpyrrolidone [PVP]), sodium hydroxide [NaOH], and double distilled deionized water. Antibacterial activity is assessed on representative Gram-negative (Escherichia coli) and Gram-positive (Streptococcus spp.) bacteria against three treatment protocols: AuNPs alone, green laser irradiation (532 nm) alone; and combined AuNP–laser treatment. By integrating synthesis medium, physicochemical properties and biological responsiveness, this paper aims to elucidate the relationship of nanoparticle–laser synergy to the development of PLAL-derived AuNPs as efficient agents for laser-enhanced antimicrobial treatment.

MATERIALS AND METHODS

Materials

Ablation targets for the synthesis of gold nanoparticles were conducted on high-purity gold metal plates (99.999%). Laser ablation was performed in three different aqueous media: double-distilled deionized water (DDDW), sodium hydroxide (NaOH) aqueous solution, and polyvinylpyrrolidone (PVP) aqueous solution with an average molecular weight of approximately 40,000 g/mol. All chemicals were of analytical grade and were used as received without further purification. Bacterial strains of Escherichia coli (Gram-negative) and Streptococcus spp. (Gram-positive) were taken from a licensed microbiology laboratory. The strains were maintained on nutrient agar media under sterile laboratory conditions and cultured on a regular basis before antibacterial testing.

Synthesis of Gold Nanoparticles by Pulsed Laser Ablation in Liquid (PLAL)

Gold nanoparticles (AuNPs) were synthesized using the pulsed laser ablation in liquid (PLAL)

technique. In this procedure, a gold plate was placed at the bottom of a glass container filled with one of the selected liquid media (DDDW, NaOH, or PVP). The surface of the gold target was irradiated using a pulsed Nd:YAG laser operating at a wavelength of 1064 nm.

The laser parameters were fixed as follows: pulse energy of 600 mJ, pulse duration of 10 ns, repetition rate of 6 Hz, and a focal spot diameter of approximately 3.5 mm on the target surface. Upon laser irradiation, metallic species were ejected from the target surface and rapidly cooled and condensed within the surrounding liquid, leading to the formation of a stable colloidal suspension of gold nanoparticles.

The ablation time was adjusted to obtain colloidal suspensions with concentrations of 100, 200, and 300 µg/mL, which were subsequently used in the antibacterial experiments. After synthesis, the nanoparticle suspensions were collected and stored in amber glass vials at room temperature to minimize undesired photo-induced effects [3,4].

Characterization of Gold Nanoparticles

The structural, morphological, and optical properties of synthesized AuNPs were systematically characterized by complementary analytical techniques. Transmission electron microscopy (TEM) was used to characterize nanoparticle morphology, dispersion state, and size distribution. X-ray diffraction (XRD) was carried out to determine the crystalline structure and phase composition of the nanoparticles.

UV–Visible spectrophotometry in the wavelength range of 300–800 nm was conducted to analyze the surface plasmon resonance (SPR) behavior of the nanoparticles and to estimate the optical band gap energy. Characterization revealed the formation of crystalline gold nanoparticles with a face-centered cubic (FCC) structure. Variations in SPR peak position and intensity were observed depending on the synthesis medium and the physicochemical properties of the nanoparticles.

Preparation of Bacterial Suspensions

Fresh colonies of E. coli and Streptococcus spp. bacteria were extracted from nutrient agar plates and suspended in sterile physiological saline solution. The turbidity of each bacterial suspension was adjusted to the 0.5 McFarland standard, corresponding to an approximate bacterial concentration of 1×10^8 CFU/mL. This standardization ensured consistent bacterial density across all antibacterial assays and experimental conditions.

Antibacterial Assays

Antibacterial activity was determined by the method of agar well diffusion. Mueller–Hinton agar plates were uniformly inoculated with standardized bacterial suspensions. Sterile wells were filled with 30 µL AuNP suspensions (100, 200, 300 µg/mL), which were prepared in each colloidal medium (NaOH, PVP, and DDDDW). The plates were incubated at 37 °C for 24 h and their diameters were measured in mm using a digital Vernier caliper. Antibacterial activity was determined by mean ± SD (standard deviation). For E. coli, the average inhibition zones were 16 ± 2 mm for NaOH-based AuNPs, 15 ± 2.65 mm for PVP-based AuNPs, and 12 ± 1 mm for DDDDW-based AuNPs. Inhibition zones (NaOH, PVP, and DDDDW) of 12 ± 1 mm, 13.33 ± 0.58 mm and 13.33 ± 1.15 mm for Streptococcus spp. were obtained.

Laser Irradiation Procedure (Photothermal / Plasmonic Treatment)

The laser irradiation protocol (e.g., photothermal/plasmonic treatment). Optical excitation was investigated to explore its effect on antibacterial behavior by using a green continuous-wave laser for the irradiation of bacterial suspensions using AuNPs at 532 nm wavelength with 300 mW of output power as a standard procedure. The laser beam was set perpendicular to the sample surface during irradiation for one and five minutes. Control experiments were performed using laser irradiation alone and AuNPs alone to distinguish between individual and combined effects. The wavelength of 532 nm was chosen because it overlapped with the surface plasmon resonance (SPR) region of the synthesized AuNPs, creating enhanced electromagnetic fields and localized photothermal heating at the surface of nanoparticles.

Evaluation of the Bacterial Viability

After completion of the respective treatments, the bacterial suspensions were transferred into 96-well microplates and incubated at 37 °C to evaluate their viability. Bacterial viability was calculated by observing the optical density (OD: 405 nm) exactly after treatment (0 h) and 24

h of incubation. Changes in the OD value were interpreted as a reduction of viable bacterial cells. The combination of AuNPs and 532 nm laser irradiation led to the biggest decrease of OD, verifying a strong synergistic photothermal/ photodynamic antibacterial effect [8].

Statistical Analysis

All experiments were performed in triplicate, and the results are presented as mean ± standard deviation. Statistical analysis was carried out using one-way analysis of variance (ANOVA) to assess differences among experimental groups. A p-value of less than 0.05 was considered statistically significant [9,10].

RESULTS AND DISCUSSION

X-Ray Diffraction (XRD)

Gold nanoparticles prepared by pulsed laser ablation in liquid (PLAL) with the use of different media, such as NaOH, PVP and DDDW were analyzed through X-ray diffraction (XRD) and the crystal structure and phase purity of the samples were determined. Fig. 1 displays the corresponding diffraction patterns and the quantitative XRD parameters such as peak positions, interplanar spacings, full width at half maximum (FWHM) and crystallite sizes are given in Table 1. Fig. 1 depicts that the diffraction peaks of all samples are quite clearly distinct, at 2θ values of approximately 38°, 44°, 64°, and 77°, which can be indexed to (111), (200), (220) and (311) crystallographic planes of face-centered cubic (FCC) gold. These reflections are strongly compatible with the typical JCPDS reference cards (Nos. 96–901–2954 to 96–901–2965), which confirms the formation of phase-pure crystalline AuNPs with no detectable phase-disposing contaminants present. The experimentally determined interplanar spacings (d_{hkl},exp) given in Table 1 closely match the

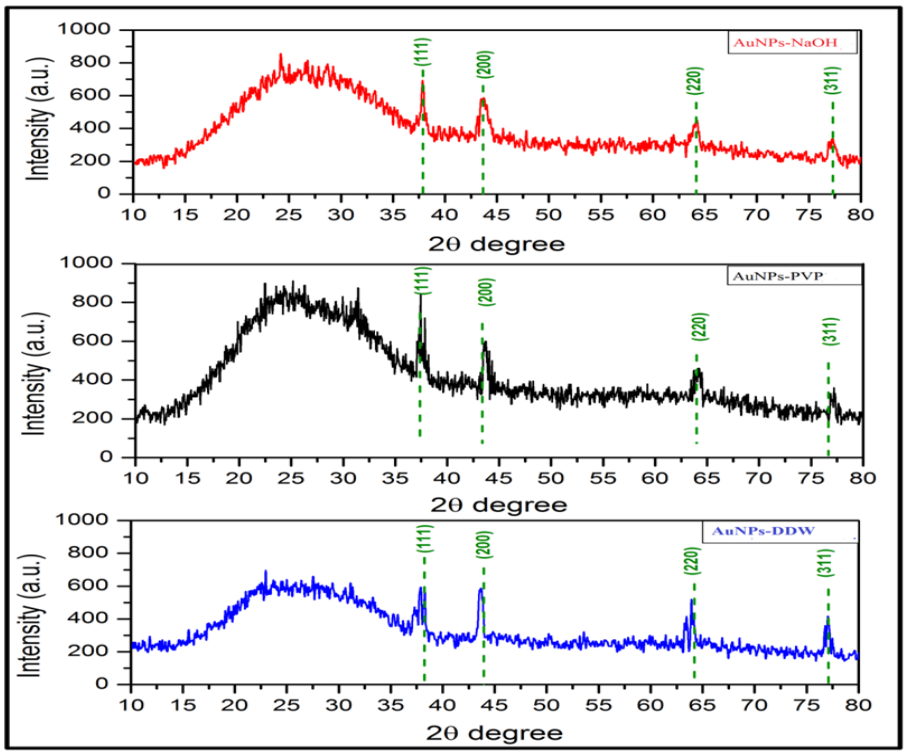

Fig. 1. X-ray diffraction (XRD) patterns of gold nanoparticles synthesized by pulsed laser ablation in liquid (PLAL) using different media: (a) NaOH, (b) PVP, and (c) double-distilled deionized water (DDDW). All samples exhibit characteristic diffraction peaks at 2θ ≈ 38°, 44°, 64°, and 77°, corresponding to the (111), (200), (220), and (311) planes of face-centered cubic (FCC) gold (JCPDS card Nos. 96-901-2954 to 96-901-2965). Variations in peak intensity and broadening reflect differences in crystallite size and crystallinity induced by the synthesis medium.

specified standard values (d_{hkl},std), confirming a high crystallographic resolution with minimal lattice distortion. Nanoscale size influences are likely responsible for minor differences between the samples, in addition to the leftover lattice strains due to the rapid quenching process characteristic of PLAL synthesis. Crystallite sizes predicted by Scherrer's equation (Table 1) strongly depend on the preparation medium. NaOH synthesized AuNPs also exhibit the lowest crystallite sizes among the materials, especially on the dominant (111) plane (~18.8 nm), as indicated by the high FWHM values recorded in Fig. 1, which can be correlated with peak broadening that occurs with the lowering of crystalline domain size and increased microstrain of the nanohalm. On the other hand, PVP AuNPs exhibit higher crystallite sizes at about 19.7 nm (Table 1) for the (311) plane, and narrower diffraction peaks in Fig. 1 in comparison, which reflects better crystallinity and stabilization by the polymeric medium. DDDW-based AuNPs present intermediate crystalline sizes, which is indicative of comparatively lower nucleation and growth control. In addition, the strong (111) reflection intensity visible in Fig. 1, along with the quantitative results presented in Table 1, indicates favoured orientation throughout this plane, which is aligned with gold nanoparticles and is correlated with higher surface stability. Importantly, the reduced crystallite size of these NaOH-based AuNPs is correlated with a larger surface to volume ratio for these compounds, and thus reflects favorably in their superior antibacterial performance that was revealed at subsequent biological evaluations. Therefore, the quantitative and qualitative XRD data displayed in Fig. 1 and Table 1 effectively reveals that liquid medium used in PLAL preparation considerably governs the crystallinity, crystallite size and structural nature of AuNPs.

Fourier Transform Infrared Spectroscopy (FTIR)

FTIR (Fourier Transform Infrared Spectroscopy) was used to determine the surface chemistry and

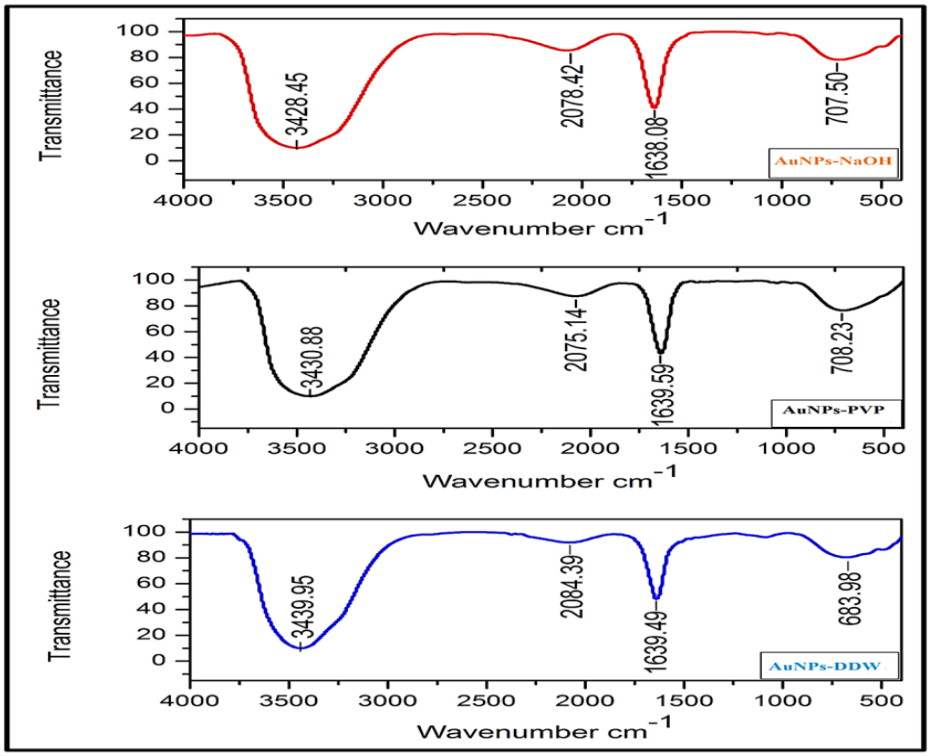

Fig. 2. Fourier transform infrared (FTIR) spectra of AuNPs synthesized via pulsed laser ablation in liquid (PLAL) in different aqueous media (NaOH, PVP, and DDDW), illustrating the surface functional groups involved in nanoparticle stabilization.

identify the functional groups originating from the synthesis media that contribute to nanoparticle stabilization in the synthesized AuNPs. FTIR analysis is extremely valuable to investigate the molecular interactions between the nanoparticle and medium which greatly influence colloidal stability and dispersion pattern. The FTIR spectra of AuNPs prepared under specific aqueous conditions

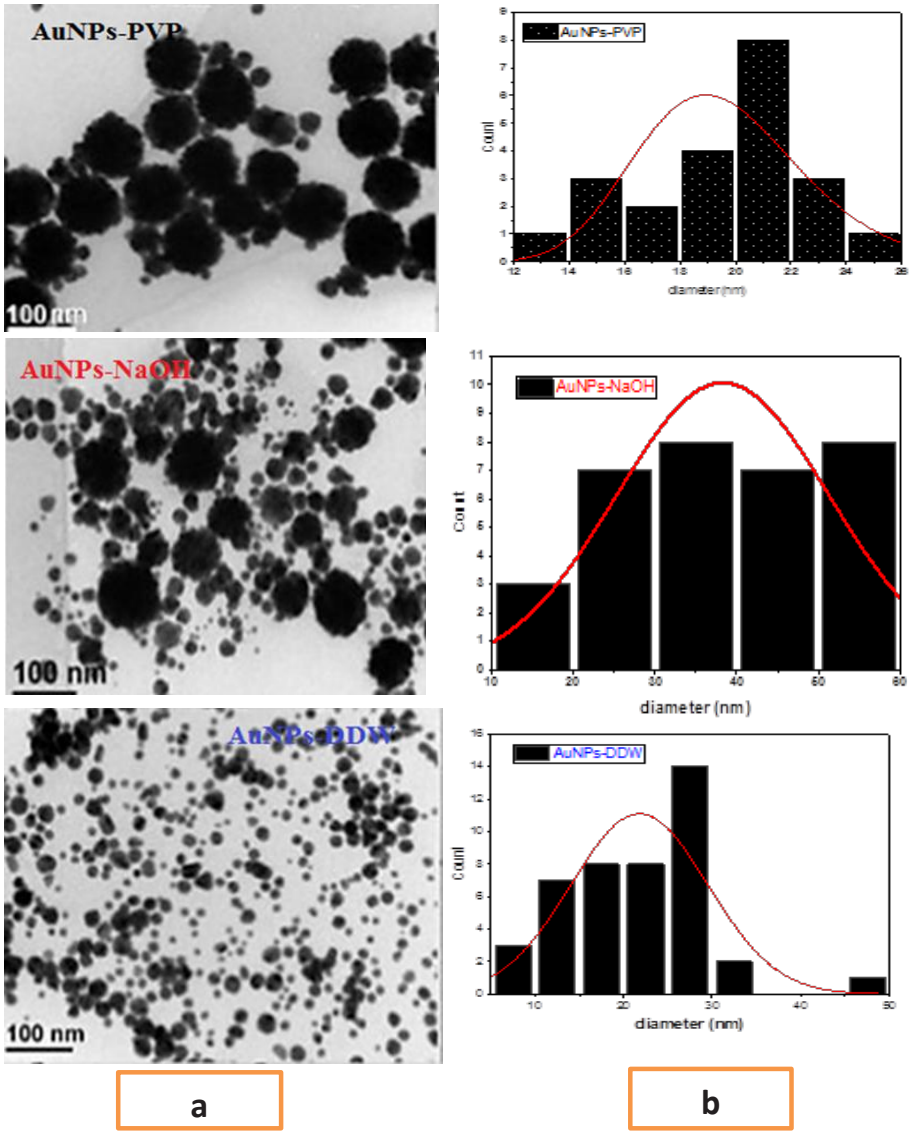

Fig. 3. TEM results of AuNPs obtained at different liquids (a) TEM images and (b) the particle size distribution.

Table 1. Average particle size of AuNPs synthesized in different media based on TEM analysis.

Sample	Minimum Diameter (nm)	Maximum Diameter (nm)	Average Diameter (nm)
AuNPs–NaOH	9.0	100.0	35.9
AuNPs–PVP	4.5	100.0	38.98
AuNPs–DDDW	6.0	100.0	25.6

(AuNaOH, AuPVP, and AuDDDW) at a range of wavenumber 4000–400 cm^{-1} are reported in Fig. 2. There is a band of absorption that is spread around 3428–3439 cm^{-1} in the total sample, which is attributed to the stretching vibrations by O–H. In the adsorption region of both adsorbents and solute compounds, surface activity is low by at least a factor of 1, with weak bands of absorption at the limit of 2500–2000 cm^{-1} in the region: a weak absorption band corresponding to (but not necessarily exclusively to) stretching vibrations of triple bonds C≡C and C≡N, arising from leftovers of organic species or (polymer fractions) in the liquid during the laser ablation process. Although these bands are small in strength, their appearances might be indicative of interface between AuNPs and organic compounds produced or liberated in PLAL. The absorption characteristics of the region of 1700–1500 cm^{-1} are due to C=O stretching vibrations that correspond with carbonyl groups. These groups belong to the organic stabilizers, polymer chains (especially for PVP), the oxidized surface species and are reported to engage in weak chemical or electrostatic bonds with gold surfaces to cause a stabilization advantage on the colloidal surface. Furthermore, the vibrational modes associated with C–H bending and other skeletal vibration of organic compounds are very noticeable in the range 1000–500 cm^{-1} of the fingerprint region. These bands additionally demonstrate that surface-bound organic species have been discovered as capping agents to AuNPs. Moreover, FTIR spectra from all materials exhibit the same overall profiles, with only subtle changes in peak positions and different intensities based on the synthesis medium. Those spectral shifts

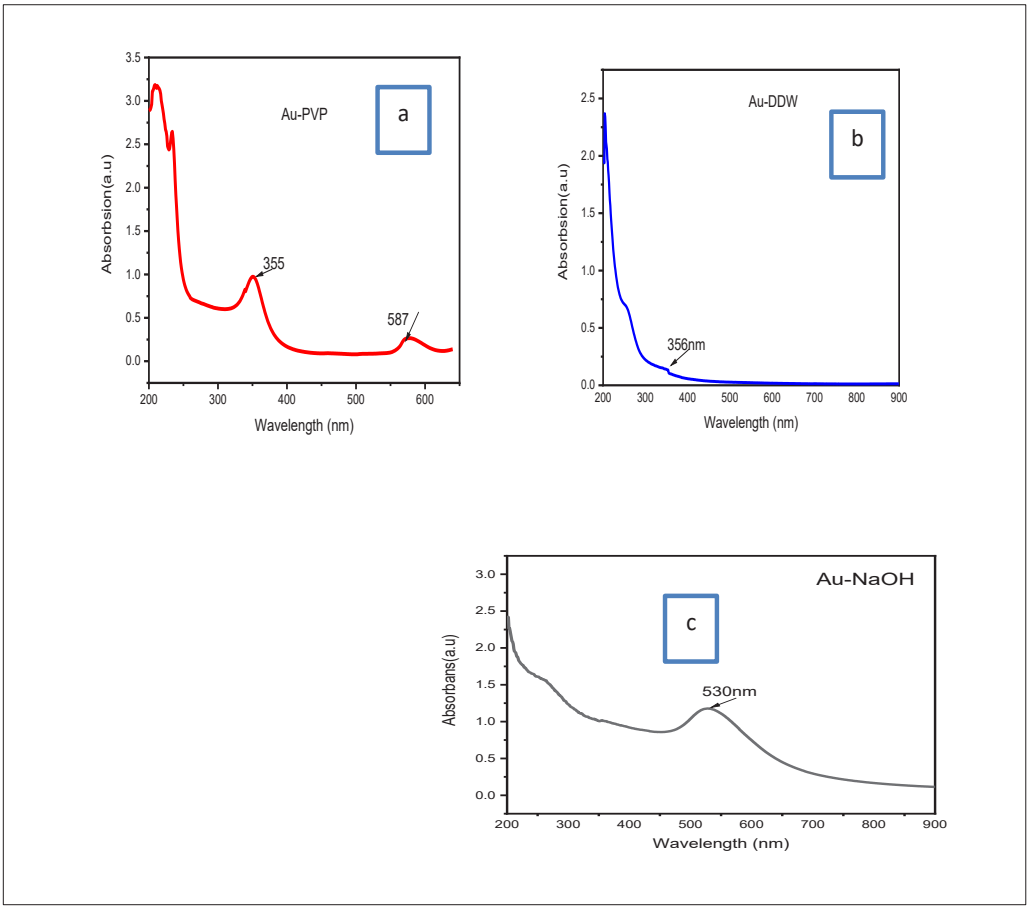

Fig. 4. UV–Visible absorption spectra illustrating the surface plasmon resonance (SPR) behavior of gold nanoparticles synthesized by pulsed laser ablation in liquid (PLAL) using different aqueous media: (a) PVP, (b) double-distilled deionized water (DDDW), and (c) NaOH.

are often due to variation in the binding context and level of interaction between the functional groups and the surface of the nanoparticle. These interactions are critical for the prevention of particle agglomeration and the stability of the colloidal dispersions. Thus, the FTIR results provide robust evidence of hydroxyl, carbonyl, and other organic functional groups in the synthesized AuNPs. These results further underline the suitability of PLAL preparation route, where medium-produced or naturally occurring organics serve as surface stabilizing agents, eliminating the requirement of added chemical modifiers; consistent with green and contamination-free

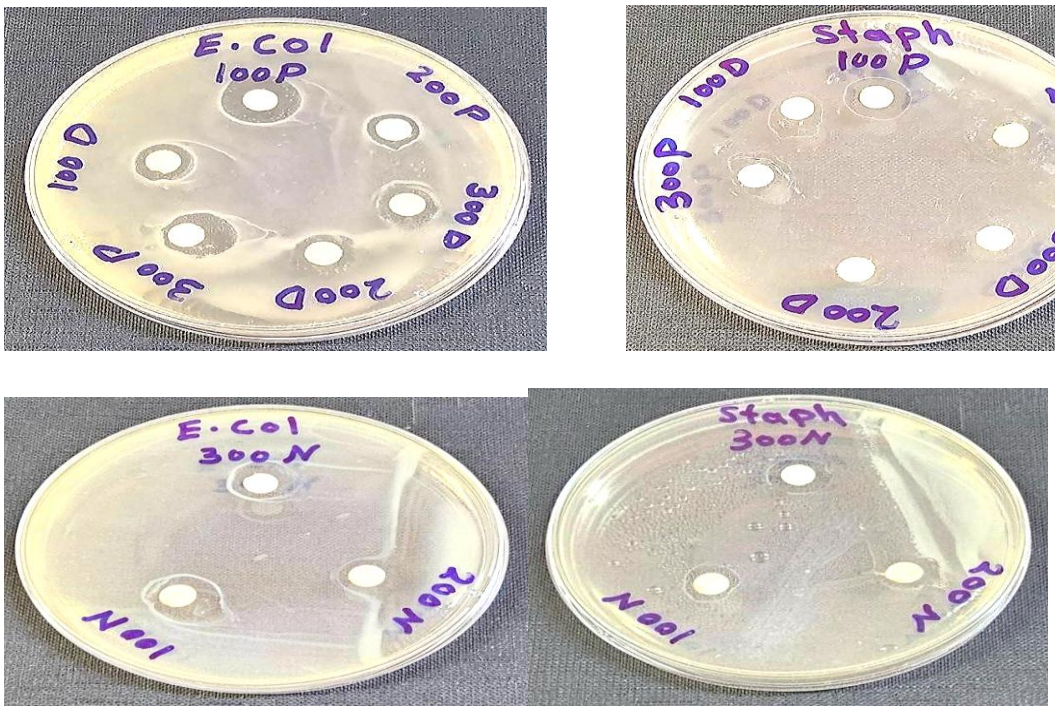

Fig. 5. Inhibition zones of Au NPs at the colloidal solutions (Au-PVP, Au-DDDW and Au-NaOH).

Table 2. Results of the biological application.

0			Streptococcus		
Concentration (μgml^{-1})	Medium	Inhibition zone (mm)	Concentration (μgml^{-1})	Medium	Inhibition zone (mm)
100	AuNP-PVP	15	100	AuNP-PVP	14
200	AuNP-PVP	10	200	AuNP-PVP	13
300	AuNP-PVP	14	300	AuNP-PVP	13
100	AuNP-DDW	11	100	AuNP-DDW	14
200	AuNP-DDW	12	200	AuNP-DDW	14
300	AuNP-DDW	13	300	AuNP-DDW	12
100	AuNP-NaOH	16	100	AuNP-NaOH	12
200	AuNP-NaOH	12	200	AuNP-NaOH	11
300	AuNP-NaOH	14	300	AuNP-NaOH	13

nanoparticle synthesis approaches.

Surface Plasmon Resonance (SPR) Analysis of AuNPs

The optical properties and surface plasmon resonance (SPR) performance of the synthesized gold nanoparticles AuNPs were explored by UV–Visible spectroscopy. The absorbance spectra obtained from AuNPs synthesized in various liquid media including polyvinylpyrrolidone (PVP), double-distilled deionized water (DDDW), sodium hydroxide (NaOH) are illustrated in Fig. 3. (a–c). The appearance of the characteristic SPR absorption bands demonstrates the successful formation of AuNPs, including the effect of the synthesis medium on the size, morphology of the nanoparticles and the surface environment. (Fig. 3.a) indicates that AuNPs prepared in the PVP medium display two polar absorption features oriented at approximately 355 nm and 587 nm. Spectra at 587 nm are characteristic of the SPR resonance of AuNPs indicating the deposition of plasmonically active particles. This increased absorption peak around 355 nm can be ascribed to the interband transitions of gold, and/or the interfaces or electronic interaction of PVP polymer chains with the nanoparticle surface. These interactions can modify the local dielectric environment resulting in a broadening as well a red shift of the SPR band corresponding to the formation of nanoparticles of higher size and polymer stabilization. The AuNPs synthesized in DDDDW (Fig. 3b), however show a blue-shifted absorption band around 356 nm, and the visible field shows no significant SPR peak. Such behaviour is indicative of the presence of ultrasmall gold nanoparticles and/or residual ionic gold species whose particle sizes fall below the requirement for a strong plasmonic oscillation. There are no stabilizers in the DDDDW media, so the controlled size of particles could be weak and/or shifted, resulting in the weak plasmonic responses. A clear and symmetric SPR band at approximately 530 nm (Fig. 3c) are observed in the UV–Vis of NaOH-based AuNPs spectra. Such peak position is typical for spherical AuNPs of moderate particle size and narrow size distribution. The high-quality alkaline environment in NaOH facilitates nucleation of nanoparticles, as well as growth control leading to higher plasmonic behavior and colloidal stability compared to the DDDDW test. Taken together, the observed differences in SPR peak position, intensity, and bandwidth for the other synthesis media clearly underline the very obvious dependence of AuNPs optical properties with the surrounding liquid environment. These results correspond to the TEM and XRD and support the notion that the PLAL-synthesized AuNPs'

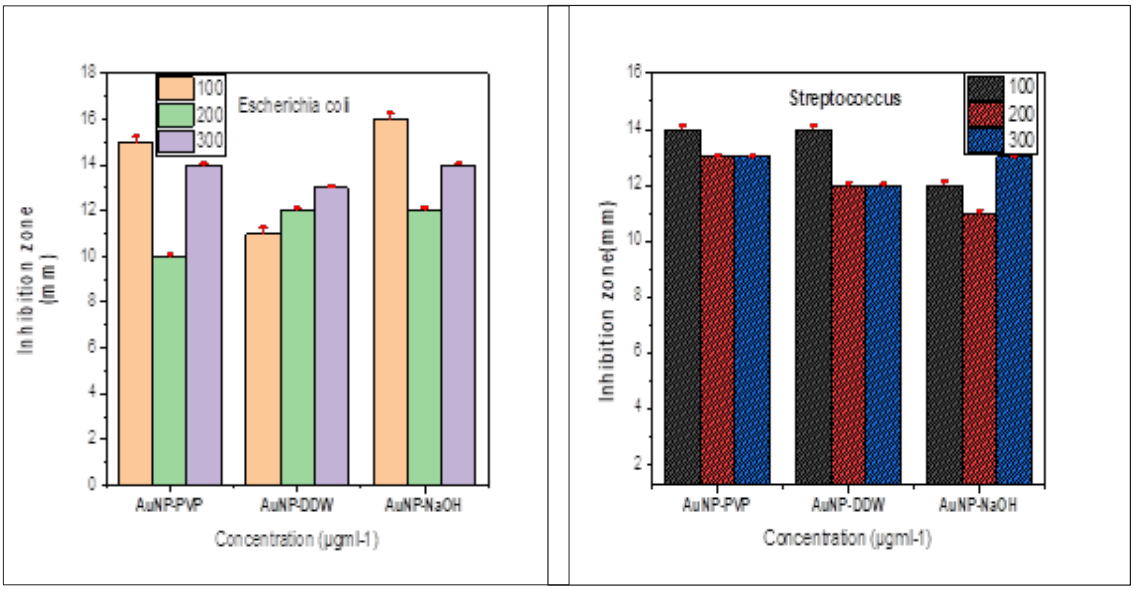

Fig. 6. Inhibition zone diameters of Escherichia coli and Streptococcus spp. exposed to gold nanoparticles (AuNPs) synthesized in different colloidal media (PVP, DDDW, and NaOH).

plasmonic behavior depends substantially on the synthesis medium that could serve in several applications, like photonics, biomedical products, or antibacterial strategies.

Transmission Electron Microscopy (TEM)

Transmission Electron Microscopy (TEM) was employed to investigate the morphology and particle size distribution of gold nanoparticles (AuNPs) synthesized in different liquid media. This technique is widely recognized for its superior spatial resolution and is commonly used to characterize the structure and size of nanomaterials with high precision .Accurate determination of nanoparticle size is essential, particularly in biomedical applications, as parameters such as shape and size directly influence cellular uptake, circulation time, and overall therapeutic performance.TEM images and particle size analysis of AuNPs synthesized in deionized double-distilled water (DDDW), sodium hydroxide (NaOH), and polyvinylpyrrolidone (PVP) are presented in Fig. 3 and summarized in Table 1. The results reveal noticeable variations in particle sizes depending on the synthesis medium. Notably, AuNPs synthesized in NaOH and PVP exhibited larger average diameters than those synthesized in DDDW. This trend is likely attributed to the influence of these liquids on nucleation and growth kinetics, where PVP may act as a capping agent and NaOH alters the pH, both impacting particle formation dynamics.

These results highlight the importance of the synthesis environment in tuning the structural characteristics of AuNPs, which in turn affects their physical and functional behavior in biomedical and catalytic applications.

Antibacterial Activity of AuNPs

Metallic nanoparticles have emerged as promising alternatives to conventional antibiotics due to their broad-spectrum antibacterial activity and reduced likelihood of inducing bacterial resistance. Among them, gold nanoparticles (AuNPs) exhibit notable antibacterial effects through direct interactions with bacterial cell walls and membranes, leading to structural damage and disruption of essential cellular processes. The antibacterial activity of the synthesized AuNPs against Escherichia coli (E. coli) and Streptococcus spp. as a function of concentration and synthesis medium is illustrated in (Figs. 5 and 6), respectively. As shown in (Fig. 4), NaOH-based AuNPs exhibited the highest inhibitory effect against E. coli, particularly at 100 µg mL^{-1}, whereas PVP- and DDDW-based AuNPs showed moderate inhibition with no clear linear dependence on concentration. In contrast, (Fig. 6) demonstrates that Streptococcus spp. displayed relatively uniform sensitivity to all AuNPs, with slightly higher inhibition zones observed for PVP- and DDDW-based nanoparticles at lower concentrations. Overall, the results presented in (Figs. 5 and 6) indicate that antibacterial efficiency depends strongly on the synthesis medium and bacterial type rather than solely on nanoparticle concentration. The diameters of the corresponding quantitative inhibition zones prepared at the different concentrations are summarized in Table 2

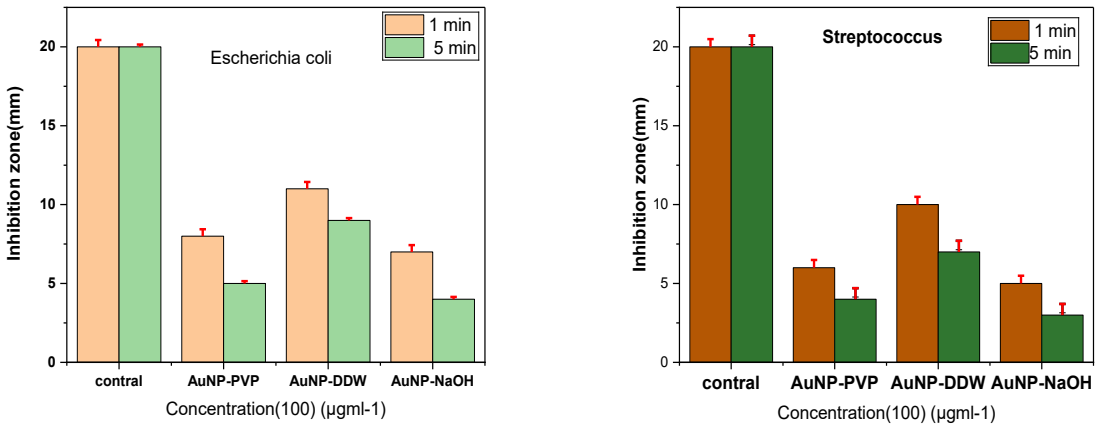

Fig. 7. Effect of 532nm and power of 300 mW laser light at deferent exposure times on the viability of Escherichia coli and Streptococcus.

and Fig. 5, to compare the antibacterial activity of AuNPs prepared in PVP, DDDW, and NaOH media.

Effect of Green Laser Irradiation on Bacterial Growth

This study is being conducted to investigate the effect of green laser irradiation on bacterial growth. Green laser irradiation alone was also evaluated for bacterial viability to differentiate between photonic action and nanoparticle-mediated effects. Escherichia coli strains and Streptococcus spp. bacterial cultures were irradiated by continuous-wave green laser (532 nm, 300 mW) without AuNPs, and allowed to cure for 1 and 5 min. Bacterial proliferation rates were evaluated promptly after exposure (0 h) and on 24 h incubation, as depicted in Fig. 7. Laser irradiation alone led to a moderate reduction in bacterial viability, with a more pronounced effect over prolonged exposure time. The negative impact upon bacterial growth may be due to photothermal stress and changes in cellular metabolism secondary to exposure to visible laser light. The inhibitory effect of laser treatment had a significantly smaller effect compared to the positive effect using AuNPs and, therefore, it was concluded that laser irradiation alone is not capable of inactivation at the treatment conditions. Visible laser irradiation imposes sublethal stress on bacterial cells that can lead to membrane breakdown and loss of enzyme activity, whereas the mechanism does not produce complete bactericidal effects independent of an external photosensitizing agent, thus strengthening earlier reports. AuNPs introduce the ability for plasmonic nano-heaters to enhance laser–bacteria interactions, thus enhancing the photothermal and photodynamic effects. The antibacterial results obtained were significant, as combined AuNPs–laser treatment presents a clear positive synergy for antibacterial effects and is better than individual AuNPs or laser irradiation. Such synergism underlines the potential of plasmonic nanoparticle-assisted photothermal therapy as a viable strategy for bacterial infections control especially under antibiotic resistance.

Statistical and Visual Interpretation of Antibacterial Activity

Descriptive statistics show similar average inhibition zone diameters for Escherichia coli and Streptococcus spp. treated with AuNPs produced in different media, with relatively small standard deviations, confirming good experimental reproducibility. One-way ANOVA indicated no statistically significant differences in inhibition zones among the synthesis media for either bacterial strain ($p > 0.05$), suggesting that variations in the liquid medium alone did not lead to changes in inhibition zones for either strain. The differences observed are still biologically relevant and interpretable, especially when considered alongside the photothermal experiments. NaOH- and PVP-based AuNPs typically showed slightly higher average inhibition values, which may be related to differences in particle size, surface chemistry, and plasmonic behavior. Such physicochemical differences become critically important under green laser irradiation, where surface plasmon resonance excitation potentiates antibacterial activity via localized photothermal and photodynamic effects. Consequently, although statistically AuNPs exhibit similar antibacterial activity across different media, their pronounced synergistic effects from laser irradiation are not captured by inhibition zone statistics alone. This illustrates the necessity of linking statistical analyses with mechanistic and photonic assessments to evaluate the true antibacterial potential of plasmonic nanoparticles.

CONCLUSION

The objective of this work was to synthesize gold nanoparticles (AuNPs) using pulsed laser ablation in liquid (PLAL) method and investigate the effect of various colloidal media (NaOH, PVP, and DDW) on their structural characteristics, optical properties and antibacterial character and to explore their application as laser-assisted antibacterial compounds. The synthesis of phase-pure AuNPs with face-centered cubic (FCC) crystal structure had also been successfully detected. As shown also in XRD and TEM analyses, the choice of the liquid medium plays a decisive role in achieving particle size, morphology and dispersion, and the sizes of NaOH- and PVP-based AuNPs were found to be relatively larger than those prepared in DDW. The optical examination showed the distinct surface plasmon resonance (SPR) behavior in the visible region, and its SPR peak position, absorption intensity and optical band gap depend very strongly on particle size and medium. With the tunable optical properties under prescribed synthesis conditions, PLAL-

fabricated AuNPs can be used for photonic and plasmonic devices. The bioassay showed that synthesized AuNPs exhibited good antibacterial activity against Gram-negative (Escherichia coli) and Gram-positive (Streptococcus spp.) bacteria. Of note, the combination of AuNPs with green laser irradiation (532 nm) demonstrated a significant synergistic antibacterial effect in particular, mediated by plasmonic photothermal induction that substantially increased the inactivation of bacteria compared to AuNPs applied alone (e.g. laser exposure or a combination of those two). Collectively, PLAL also establishes its versatility and green potential for tunable AuNPs with advanced optical and antibacterial properties. Our results thus have implications for the applicability of plasmonic AuNP-laser systems as a targeted antimicrobial strategy, especially in the realm of antibiotic resistance. Laser parameters should be further optimized along with biocompatibility studies to further improve their biomedical applications.

CONFLICT OF INTEREST

The authors declare that there is no conflict of interests regarding the publication of this manuscript.

REFERENCES

1. Global antibiotic resistance surveillance report 2025: World Health Organization; 2025 2025/10/13.
2. Naghavi M, Murray CJL, Ikuta KS, Mestrovic T, Swetschinski L, Sartorius B. Global burden of antimicrobial resistance: essential pieces of a global puzzle – Authors' reply. The Lancet. 2022;399(10344):2349-2350.
3. Prestinaci F, Pezzotti P, Pantosti A. Antimicrobial resistance: a global multifaceted phenomenon. Pathogens and Global Health. 2015;109(7):309-318.
4. Szul M. Causes Behind the Global Crisis of Increasing Antibiotic Resistance and Strategies to stop this. Polygence; 2024. http://dx.doi.org/10.58445/rars.1194
5. Davies J, Davies D. Origins and Evolution of Antibiotic Resistance. Microbiology and Molecular Biology Reviews. 2010;74(3):417-433.
6. Li Y, Yang L, Liao Y, Zhao R, Ji L, Su R, et al. Photothermal Heating-Assisted Superior Antibacterial and Antibiofilm Activity of High-Entropy-Alloy Nanoparticles. Adv Funct Mater. 2023;33(35).
7. Wang B, Chen S, Feng W, Shan X, Zhu X, Yuan R, et al. Antimicrobial Peptide-Modified Liquid Metal Nanomaterials for Enhanced Antibacterial Photothermal Therapy. Adv Eng Mater. 2024;26(12).
8. Wu G, Xu Z, Yu Y, Zhang M, Wang S, Duan S, et al. Biomaterials-based phototherapy for bacterial infections. Front Pharmacol. 2024;15.
9. Dreaden EC, Alkilany AM, Huang X, Murphy CJ, El-Sayed MA. The golden age: gold nanoparticles for biomedicine. Chem Soc Rev. 2012;41(7):2740-2779.
10. Aguilar-Garay R, Lara-Ortiz LF, Campos-López M, Gonzalez-Rodriguez DE, Gamboa-Lugo MM, Mendoza-Pérez JA, et al. A Comprehensive Review of Silver and Gold Nanoparticles as Effective Antibacterial Agents. Pharmaceuticals. 2024;17(9):1134.
11. Kelly KL, Coronado E, Zhao LL, Schatz GC. The Optical Properties of Metal Nanoparticles: The Influence of Size, Shape, and Dielectric Environment. The Journal of Physical Chemistry B. 2002;107(3):668-677.
12. Liu L, Wu W, Fang Y, Liu H, Chen F, Zhang M, et al. Correction: Liu et al. Functionalized MoS2 Nanoflowers with Excellent Near-Infrared Photothermal Activities for Scavenging of Antibiotic Resistant Bacteria. Nanomaterials 2021, 11, 2829. Nanomaterials. 2023;13(5):824.
13. Qin H, Yang Z-R, Lv N, Ma T, Du K, Xiong J, et al. pH-Induced reversible self-assembly of gold nanoparticles functionalized with self-complementary zwitterionic peptides for near-infrared photothermal antibacterial treatment. New J Chem. 2023;47(18):8661-8669.
14. Cao J, Song Z, Du T, Du X. Antimicrobial materials based on photothermal action and their application in wound treatment. Burns and Trauma. 2024;12.
15. Zhang X-F, Liu Z-G, Shen W, Gurunathan S. Silver Nanoparticles: Synthesis, Characterization, Properties, Applications, and Therapeutic Approaches. Int J Mol Sci. 2016;17(9):1534.
16. Peng Z, Royon L, Luo Y, Decorse P, Derouich SG, Bosco M, et al. Eradication of planktonic bacteria by shape-tailored gold nanoparticle photothermia. Materials Advances. 2024;5(21):8524-8533.
17. Nune SK, Chanda N, Shukla R, Katti K, Kulkarni RR, Thilakavathy S, et al. Green nanotechnology from tea: phytochemicals in tea as building blocks for production of biocompatible gold nanoparticles. J Mater Chem. 2009;19(19):2912.
18. Amendola V, Meneghetti M. Laser ablation synthesis in solution and size manipulation of noble metal nanoparticles. Physical Chemistry Chemical Physics. 2009;11(20):3805.
19. Costa DC, Fernandes M, Moura C, Miranda G, Silva F, Carvalho Ó, et al. Laser ablation in liquid-assisted synthesis of three types of nanoparticles for enhanced antibacterial applications. International Journal of Precision Engineering and Manufacturing-Green Technology. 2025;12(6):1699-1717.
20. Zhang D, Gökce B, Barcikowski S. Laser Synthesis and Processing of Colloids: Fundamentals and Applications. Chem Rev. 2017;117(5):3990-4103.
21. Sajti CL, Sattari R, Chichkov B, Barcikowski S. Ablation efficiency of α-Al_2O_3 in liquid phase and ambient air by nanosecond laser irradiation. Appl Phys A. 2010;100(1):203-206.
22. Sylvestre J-P, Poulin S, Kabashin AV, Sacher E, Meunier M, Luong JHT. Surface Chemistry of Gold Nanoparticles Produced by Laser Ablation in Aqueous Media. The Journal of Physical Chemistry B. 2004;108(43):16864-16869.
23. Gold Nanoparticles for Photothermal and Photodynamic Therapy. American Chemical Society (ACS). http://dx.doi.org/10.1021/acsomega.4c08797.s001
24. Darvish S, Budala D-G, Goriuc A. Antibacterial Properties of an Experimental Dental Resin Loaded with Gold Nanoshells for Photothermal Therapy Applications. Journal of Functional Biomaterials. 2024;15(4):100.
25. Cecotka M, Radomski P, Ziółkowski P, Tymińska A, Czerwiec K, Zieliński J, et al. Laser irradiation of human skin tissue after gold nanoparticles injection for thermal ablation processes – a combined experimental and numerical approach. Sci Rep. 2025;15(1).